1-25-2012

Application of Image Processing to Track Twin Boundary Motion in Magnetic Shape Memory Alloys

Adrian Rothenbuhler
Boise State University

Elisa Barney Smith
Boise State University

Peter Müllner
Boise State University

 DOI: 10.1117/12.907070

Application of Image Processing to track Twin Boundary Motion in Magnetic Shape Memory Alloys

Adrian Rothenbuhler, Elisa H. Barney Smith and Peter Müllner

Boise State University, 1910 University Drive, Boise, ID 83725
EBarneySmith@BoiseState.edu

ABSTRACT

Materials scientists make use of image processing tools more and more as technology advances and the data volume that needs to be analyzed increases. We propose a method to optically measure magnetic field induced strain (MFIS) as well as twin boundary movement in Ni_2MnGa single crystal shape memory alloys to facilitate spatially resolved tracking of deformation. Current magneto-mechanical experiments used to measure MFIS can measure strain only in one direction and do not provide information about the movement of individual twin boundaries. A sequence of images captured from a high resolution camera is analyzed by a boundary detection algorithm to provide strain data in multiple directions. Subsequent motion detection and Hough feature extraction provide quantitative information about the location and movement of active twin boundaries.

Keywords: Motion detection, edge detection, Hough transformation, twin boundaries, magnetic shape memory alloy, Ni_2MnGa single crystal

1. INTRODUCTION

Recent advances in imaging and computing technology have led to an increase in the use of image processing for automated material characterization in the field of Materials Science. This paper discusses how image processing can be used to visualize twin boundaries in a magnetic shape memory alloy (MSMA) which are usually only visible under polarized light. Furthermore, the magnetic field induced strain (MFIS) of the sample can be measured optically without constraining the sample. The proposed technique can be used to characterize Ni_2MnGa single crystals as well as to quantify how well they work as a shape memory alloy.

MSMAs are special materials with reversible plastic strain accomplished by the reorientation (or rotation) of a magnetic field relative to the sample. MSMAs can produce MFIS as large as 10% with fast response times.[1–3] Potential applications range from actuators and sensors to small power generation devices. The MFIS is facilitated through the magnetic-field-induced motion of so called twin boundaries. A twin boundary is a symmetrical crystal interface where one side mirrors the other side of the crystal structure. Twin boundaries move in response to an external force such as a magnetic field or mechanical stress. When investigating MSMAs, it is of great interest to find the maximal MFIS, which is the expansion of the sample when a magnetic field is applied. Furthermore, the twin microstructure has a dramatic impact on the performance of MSMAs.[4–7] However, in situ visualization of twin boundary motion during magnetic field rotation is usually not reported. The study and understanding of twin boundaries are vital parts of MSMA research.

Fig. 1 shows two twin boundaries as symetrical interfaces. As the strength of the applied magnetic field increases, the magnetic moments associated with each unit cell within the crystal lattice start reorienting themselves in the direction of the applied magnetic field. The magnetic anisotropy energy drives the twin boundaries to move to the side, causing a shape change. As mentioned above, twin boundaries are normally only visible under polarized light and under particular illumination conditions.[4] Electron backscatter diffraction (EBSD) experiments are usually used to identify twin boundaries. However, these experiments are very laborious and can't be added to an existing experimental setting. In situ visualization of twin boundaries (e.g. in a rotating magnetic field) add another level of complexity as there are no off-the-shelf products that allow such experiments to be conducted either directly on the stage of a microscope or to put the optical imaging equipment into a rotating magnetic field setup. The proposed method uses a digital high resolution camera and an image processing algorithm to simplify the experimental setup while providing information about in situ twin boundary movement as well as the MFIS. Edge detection, motion detection, and feature extraction tools are employed to provide this

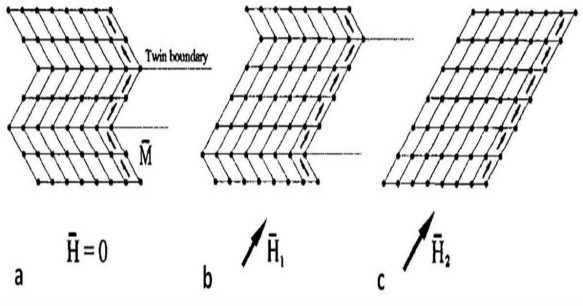

Figure 1: Crystal lattice showing the rearangement of magnetic moments causing twin boundaries to move through the lattice.[8]

information, which will be reported as a graph showing the strain (ϵ_{xx} and ϵ_{yy}) vs. the magnetic field angle. Furthermore, detected twin boundaries, maximum strain as well as the direction of the applied magnetic field will be shown on the captured image.

2. EXPERIMENTAL SETUP AND REQUIREMENTS

The experimental setup consisted of a custom built pivot mounted high-resolution camera (Lumenera Model Infinity X-21) and sample holder enclosed in an aluminum frame. For the experiments described here, the setup was put between the polepieces of an electromagnet with variable field strength in order to perform MFIS experiments. Alternatively, permanent magnets can be used. Since the camera is rigidly attached to the sample holder and spun together with the sample, the rotational motion is not captured. Instead, the camera records only the sample's shape change.

Strain is defined as the change of length divided by the initial length. Calculations for a sample's strain therefore require detection of the sample's rectangular area that is facing the camera. Once the image processing software detects all edges, the area can be identified and strain can easily be calculated using the initial and current dimensions. Twin boundary detection, however, is not as trivial. The experimental setup described above has spatial constraints that prohibit the incorporation of polarized light. Static twin boundaries can therefore not be seen by the eye or camera. However, since this is an in-situ experiment and twin boundaries induce strain as they move through the sample, their location is found at the interface between the part of the sample that moved and that which didn't. A motion detection algorithm is therefore required to detect the moving part of the sample. Since twin boundaries are always depicted as straight lines, employment of a Hough transformation, which is a line detection algorithm, is sufficient to track the location and direction of movement of individual twin boundaries.

3. SAMPLE BOUNDARY DETECTION

Sample boundary detection is needed for both strain analysis and twin boundary detection. Fig. 2a shows the sample as seen by the camera. The sample holder to which the sample was glued can be seen on the left side. Since the only motion captured by the camera is due to MFIS, a signifficant amount of image processing can be eliminated by applying a region of interest (ROI). Simplification of the image processing algorithm is especially important when processing a large amount of high resolution images. The user is required to define the ROI only for the first image, making sure that the entire sample but not the sample holder is selected. The ROI must completely black out the sample holder and at the same time leave enough space around the sample to allow its expansion to be detected (as seen in Fig. 2b). The sample boundary detection algorithm now only has to distinguish between the sample and the background. Once defined, the ROI is applied to every subsequent image for sample boundary detection. This simple procedure is possible because the sample holder doesn't move with respect to the camera.

One approach to sample boundary detection is to first convert the original color image to an HSV (Hue, Saturation, and Value) image. All three HSV image planes are used to detect edges using average filtering

and subsequently applying a Sobel edge detection filter. Combining the individual results from the three HSV matrices results in edges that are more pronounced than applying a Sobel filter to a gray scale image. Finally, morphological opening followed by morphological closing is performed to first remove noise along the sample's edge and then to close small holes to make the sample boundary smooth. However, this approach showed some inaccuracies (especially during twin boundary movement) and only worked well with the sample seen in Fig. 2a. With a different sample or adjusted lighting, the algorithm will cause the strain analysis to report highly inaccurate numbers. This is because the described approach is too sensitive to changes in the sample's surface. Furthermore, it was found that the gradient between the sample and the background is very small. For the algorithm to accurately detect the samples shape it is important to have an image that shows a clear difference between the sample and the background, thus having a large gradient.

Contrary to most image processing applications, this experiment is not constrained to certain parameters. Background and lighting can be adjusted to facilitate image processing. To increase the gradient, the background of the sample holder needs to be significantly darker, which was done here by applying black tape. Using an LED controller, the LED light source can be dimmed to further enhance image quality. This leads to the a priori information that the sample holder has a background that is signifficantly darker than the polished or etched metallic sample surface. With this information we can further simplify the edge detection algorithm while making it more efficient. Instead of processing HSV image planes and applying a Sobel filter, applying a global threshold to a gray scale image is sufficient. The threshold needs to be slightly above the average gray scale value of the background, which can be found experimentally. This simple process is very effective. Polishing or etching artifacts might still show up as small dark pits, but they are easily eliminated by performing a flood fill on the detected sample as well as performing the same morphological operations as above to smooth the edges. An adaptive threshold was considered but did not show any advantages over a global threshold.

Fig. 2c has a much larger gradient between the sample and the background than Fig. 2a, leading to a more efficient sample boundary detection algorithm. As seen in Fig. 2d, the sample is correctly and accurately detected and its boundaries are outlined in red. Figs. 2c and 2d both show the same sample as in Figs. 2a and 2b but were captured at a later time with different lighting, darker background and different zoom setting of the camera's zoom lens, causing the optical illusion of different sample dimensions.

4. STRAIN ANALYSIS

Strain is a unitless description of a relative dispacement and is an important characterization tool in plastic deformation experiments. Current magneto-mechanical experiments measure strain only in one direction. Using a high resolution camera and image processing, multi-dimensional strain measurements are easily performed and, in fact, do not constrain the sample mechanically. Here, strain is measured in two dimensions (x and y) by laying a grid over the image with the grid lines terminated at the sample's boundary using the detected sample boundary as a mask. Grid lines are placed every N pixels apart, with N specified by the user. Each horizontal and vertical line of the grid provides information about the sample's size. By finding the longest lines, the maximum strain can easily be calculated, but each line can also be used for a local strain or average strain calculation. Since strain is unitless, the length of each line, which is measured in pixels, does not need to be converted into another unit. The line lengths of the very first frame are used as the initial sample dimensions. Fig. 3 shows the sample with the grid overlay. The lines corresponding to the maximum length in both x and y direction are marked red.

5. TWIN BOUNDARY DETECTION

Active twin boundaries can be found by identifying the interface of the part of the sample that moved and the part which didn't. This requires a motion detection algorithm, which is based on the difference of two images I_k, where k is the frame number of an image sequence and n is a particular point.[9] This results in the difference matrix

$$d_k[n] = I_k[n] - I_{k-1}[n]. \tag{1}$$

Background noise from the camera and/or the environment prevents any two images from being exactly the same. The majority of this noise can be supressed by applying a 3x3 convolutional averaging filter to the difference

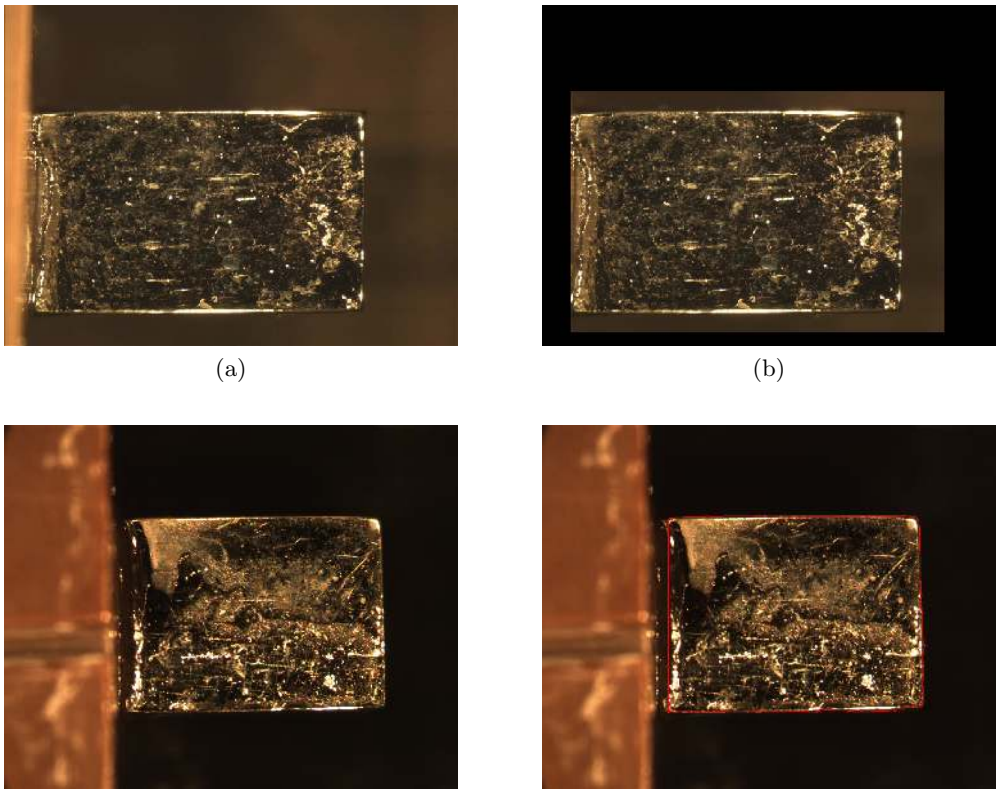

(a) (b)

(c) (d)

Figure 2: (a) Original sample image as seen by the camera (b) Region of Interest (ROI) mask applied to the original image (c) New sample set with same sample but different background color (d) Result from the edge detection algorithm. The edges are much more accurate with the use of a darker background than with the background in Fig. 2a.

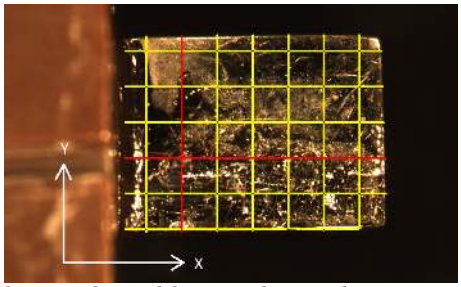

Figure 3: Grid overlay for strain analysis. The red lines indicate the maximum dimension in each direction. The measured lines are compared to the initial length lines of the sample to calculate strain.

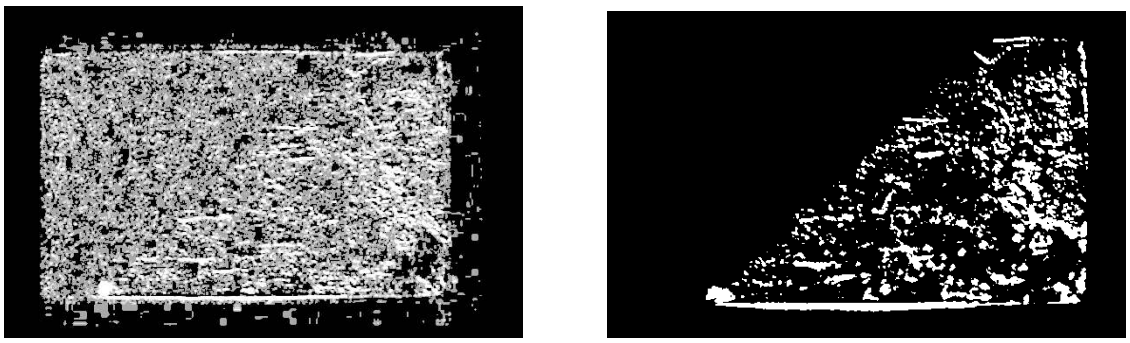

(a) (b)

Figure 4: (a) Contrast enhanced image of basic motion detection with a lot of background noise present. (b) Improved motion detection obtained by applying a noise filter and thresholding algorithm to difference matrix.

matrix d_k. In addition to that, thresholding the difference matrix to remove the remaining noise will reveal the true motion.[9] The squared difference matrix $(d_k)^2$ ensures that negative values (differences) will become positive and makes them subject to thresholding with a positive constant. Thresholding the difference matrix $d_k[n]$ classifies a point n as either moving (M) or stationary (S) and can mathematically be expressed as

$$d_k^2[n] \underset{S}{\overset{M}{\gtrless}} \sigma. \tag{2}$$

Fig. 4a shows the result from applying basic motion detection (1) to a set of two consecutive images from our sample set. Background noise is dominant in Fig. 4a, making it impossible to detect which part of the sample actually moved. Also, the whole sample is visible in the visualized difference matrix, indicating that there is a lot of jitter on the sample surface. An ideal value for the threshold σ was found empirically by slowly increasing σ until no motion due to background noise was observed. The result, as shown in Fig. 4b, is satisfying and was achieved with $\sigma = 3500$. The visible triangular part of the sample is the part that moved due to twin boundary motion. Furthermore, the slanted side (at an angle of approximately 45° relative to the x axis) indicates the location of a twin boundary, which is the twin boundary closest to the stationary sample holder.

From Fig. 4b we can deduce that the location and orientation of a single twin boundary can be found by performing motion detection and applying a least squares fit through the slanted side that is not part of the sample's edges. However, it is possible that multiple twin boundaries move through the sample simultaneously. In this case, we need to extract more information from the difference matrix d_k. This can be done with the Hough transform line extraction technique. Based on the parametric line equation

$$\rho = xcos(\theta) + ysin(\theta), \tag{3}$$

the Hough transform finds all ρ and θ line parameters for all possible lines between any two points. The parameters that occur most frequently indicate a high probability that lines are present.[10] Depending on the arrangement of the points that were classified as moving, one might argue that the detected lines are simply due to a coincidental allignment of these points and do not depict the presence of a twin boundary. However, when looking at the Hough accumulator plot in Fig. 5a, showing all line parameters that were found for an individual frame, one can see three peaks at an angle of 45°, one at 0°, and one at approximately 90° marked with black boxes. The curves show where line parameters were found in the ρ and θ space and the peaks indicate the presence of a line. The three peaks at 45° are due to twin boundary movement and the remaining peaks (0°, 90°) due to the sample's edges. In Ni_2MnGa, twin boundaries are of the {101} type and are inclined at an angle of approximately 45° relative to the horizontal sample axis. We can therefore conclude that the lines found at 45° are not caused by coincidental allignment and are in fact twin boundaries. We underline this hypothesis further with Fig. 5b, which shows a 3D Hough accumulator plot. A distinct crest at 45° is seen and is only present during twin boundary movement. With this clear distinction between twin boundaries and any other detected linear artifacts, we can setup a filter that will only consider lines that fit the twin boundary criteria for this material.

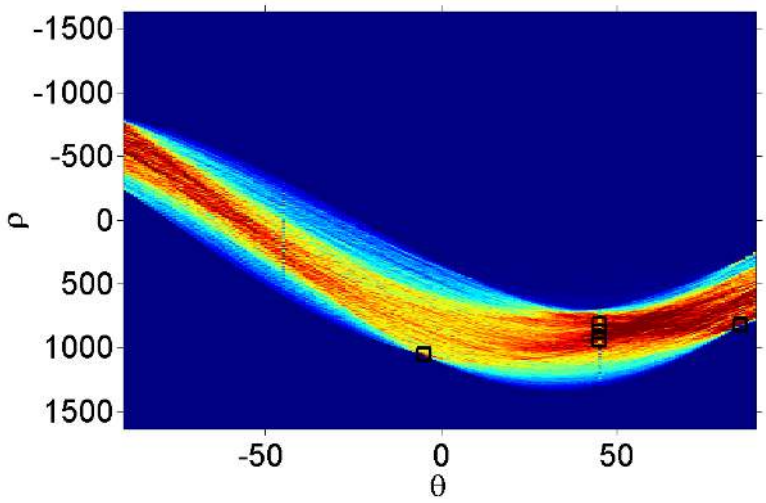

(a)

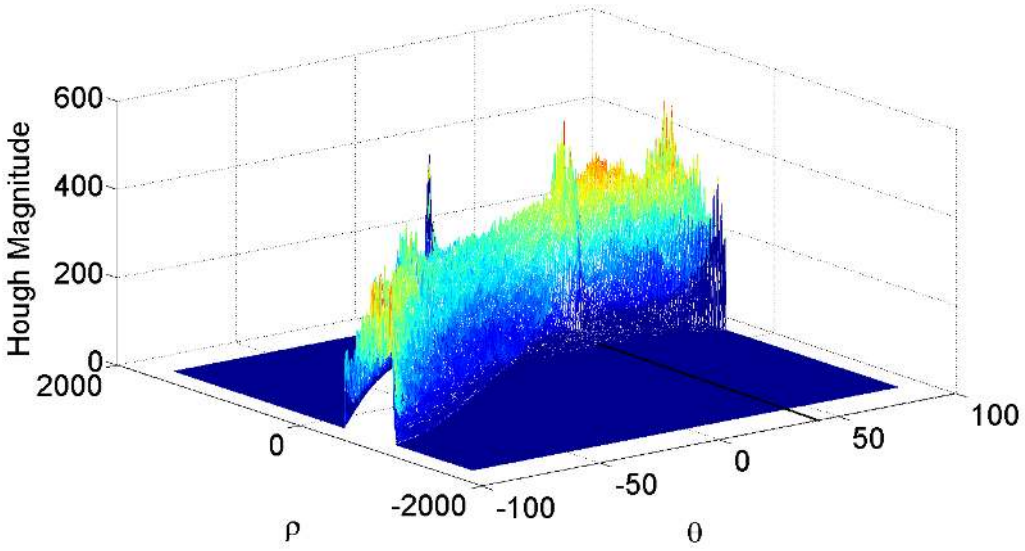

(b)

Figure 5: (a) Plot of Hough transformation accumulator. Peaks marked with black boxes indicate the location of a detected line. (b) 3D surface plot of Hough transformation accumulator. The peaks clearly indicate lines at 0°, 45°, and 90°.

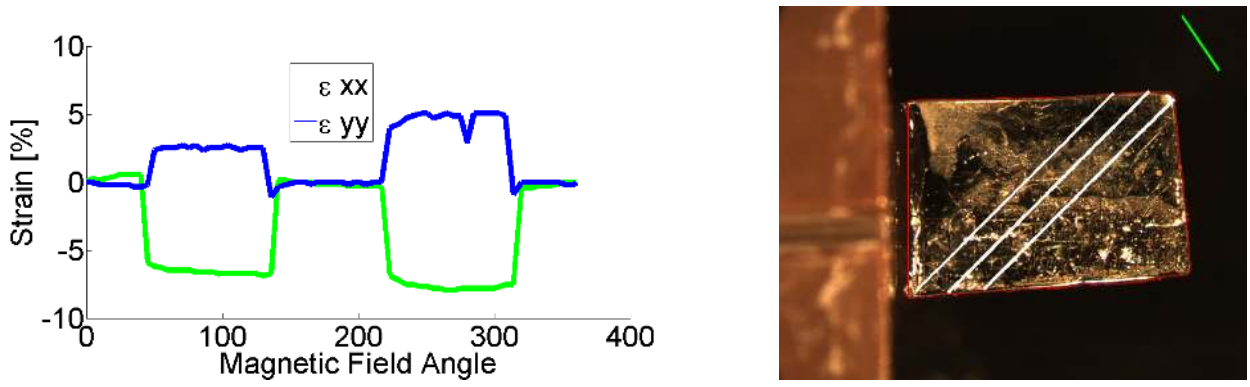

(a) (b)

Figure 6: (a) Strain analysis results. The strain vs. field angle reveals deformation events. (b) Twin boundary detection results. The detected twin boundaries are drawn as white lines and the orientation of the magnetic field is indicated by a green line.

6. RESULTS

The proposed procedure was applied to a sequence of images obtained by rotating an MSMA in a magnetic field from 0° to 360°. High resolution images were taken at a 5° interval. Fig. 6a shows the final result from the strain analysis with the maximum strain plotted against the angle of the magnetic field. The sample undergoes four shape changes from elongated along the x direction (at 0°) to compressed along the x direction and back. The transitions occur sharply at the field angles 55°, 150°, 230°, and 330°. The maximum strain option was used on purpose to show that the maximum strain of the sample is indeed within the expected range of less than 10%. When the strain was averaged over the entire grid (see section 4), the lines were smoother with no dips. Fig. 6a shows that deformation occurs in a narrow angular range and implies that tracking twin boundary motion requires a smaller rotational step size than the 5° step size employed in this study.

Fig. 6b shows the location of the detected twin boundaries on the captured image, depicted as white lines. The three twin boundaries correspond to the three peaks at 45° in Fig. 5a. Together Figs. 6a and 5a show which twin boundaries caused the majority of MFIS (plastic deformation). This will also help to get a better understanding of which areas of the sample facilitate twin boundary movement and which hinder them, possibly due to constaints from the sample holder.[11] The orientation of the magnetic field is shown in Fig. 6b as a green line, which is an important piece of information when characterizing twin boundary motion.

7. CONCLUSION

An image processing algorithm was developed to provide an experimental procedure for the automated detection of strain and twin boundary motion in MSMAs. A global threshold separates the sample from its background to extract the sample boundary. Based on this information, strain can be calculated in two dimensions for each frame of the image sequence. Using motion detection and the Hough transformation, moving twin boundaries were detected and superimposed on the original image. Although Matlab was used for the implementation of the proposed algorithm, any other platform can be used to perform strain and twin boundary analysis on MSMAs.

The experimental setup is required to have a dark background so that the thresholding algorithm can easily distinguish between the brighter sample and the darker background. Also, lighting should be adjusted to maximize contrast and reduce glare on the metallic sample surface. This study also showed that the increments at which images are taken have to be less than 5° to increase spatial resolution and to get more accurate twin boundary tracking results. It was found that the proposed algorithm was able to detect multiple twin boundaries, but reported them at incorrect locations when a high rotational step size (lower angular resolution) was used. This is probably due to the possibility that additional twin boundaries start to move between the two positions where pictures were taken and move past the starting position of the next twin boundary. It is impossible for the motion detection algorithm to correctly detect the difference between the images if a twin boundary jumps

over the starting position of the next twin boundary. This can be avoided with a low rotational step size and ensures that twin boundaries are tracked more accurately.

8. ACKNOWLEDGMENTS

We would like to thank Anita Poudel and Wayne Kreimeyer for their support and contribution building the rotation control system for this project, Phil Boysen for machining parts, Markus Chmielus and Cassie Witherspoon for their work on the mechanical setup. AR and PM acknowledge financial support from the National Science Foundation through project number NSF-DMR 1008167.

REFERENCES

[1] Ullakko, K., Huang, J., Kantner, C., and O'Handley, R., "Large magnetic-field-induced strains in Ni_2MnGa single crystals," *Applied Physics Letters* **69**, 1966–1968 (September 1996).

[2] Sozinov, A., Likhachev, A., and Ullakko, K., "Giant magnetic-field-induced strain in NiMnGa seven-layered martensitic phase," *Applied Physics Letters* **80**, 1746–1748 (2002).

[3] Murray, S., Marioni, M., Allen, S., O'Handley, R., and Lograsso, T., "6% magnetic-field-induced strain by twin-boundary motion in ferromagnetic Ni-Mn-Ga," *Applied Physics Letters* **77**, 886–888 (2000).

[4] Straka, L., Lanska, N., Ullakko, K., and Sozinov, A., "Twin microstructure dependent mechanical response in Ni-Mn-Ga single crystals," *Applied Physics Letters* **96**, 131903–131906 (2010).

[5] Müllner, P., Chernenko, V., and Kostorz, G., "Large cyclic magnetic-field-induced deformation in orthrombic (14M) Ni-Mn-Ga martensite," *Journal of Applied Physics* **95**, 1531–1536 (2004).

[6] Aaltio, I., Soroka, A., Ge, Y., Söderberg, O., and Hannula, S.-P., "High-cycle fatigue of 10M Ni-Mn-Ga magnetic shape memory alloy in reversed mechanical loading," *Smart Materials and Structures* **19** (2010).

[7] Chmielus, M., Chernenko, V., Knowlton, W., Kostorz, G., and Müllner, P., "Training, constraints, and high-cycle magneto-mechanical properties of Ni-Mn-Ga magnetic shape-memory alloys," *The European Physics Journal Special Topics* **158**, 79–85 (2008).

[8] Ullako, K., Huang, J., Kokorin, V., and O'Handley, R., "Magnetically controlled shape memory effect in Ni_2MnGa intermetallics," *Scripta Materialia* **36**, 1133–1138 (1997).

[9] Bovik, A., [*Handbook of Image and Video Processing*], Academic Press, Burlington Massachusetts (2005).

[10] Gonzalez, R. and Woods, R., [*Digital Image Processing*], Prentice Hall, New Jersey, New York (2008).

[11] Chmielus, M., Glavatskyy, I., Hoffmann, J., Chernenko, V., Schneider, R., and Müllner, P., "Influence of constraints and twinning stress on magnetic field-induced strain of magnetic shape-memory alloys," *Scripta Materialia* **64**, 888–891 (2011).